

# **SURFACE COMPLEXATION MODELING**

## **Hydrous Ferric Oxide**

**David A. Dzombak**

*Carnegie Mellon University  
Pittsburgh, Pennsylvania*

**François M. M. Morel**

*Massachusetts Institute of Technology  
Cambridge, Massachusetts*



WILEY

A Wiley-Interscience Publication

**JOHN WILEY & SONS**

New York / Chichester / Brisbane / Toronto / Singapore

*To Geoffrey D. Parfitt  
surface chemist, engineer, and educator*

Copyright © 1990 by John Wiley & Sons, Inc.

All rights reserved. Published simultaneously in Canada.

Reproduction or translation of any part of this work  
beyond that permitted by Sections 107 or 108 of the  
1976 United States Copyright Act without the permission  
of the copyright owner is unlawful. Requests for  
permission or further information should be addressed to  
John Wiley & Sons, Inc., Permissions Department, John Wiley & Sons, Inc.

*Library of Congress Cataloging in Publication Data*

Dzombak, David A., 1957-  
Surface complexation modeling: hydrous ferric oxide/David A.  
Dzombak, François M. M. Morel.

p. cm.

"A Wiley-Interscience publication."

Bibliography: p.

ISBN 0-471-63731-9

1. Ferric oxide. 2. Adsorption. 3. Surface chemistry.

I. Morel, François M. M., 1944- II. Title.

QD181.F4D96 1990

89-35596

546'.62122--dc20

CIP

9 8 7 6 5 4 3 2 1

## PROPERTIES OF HYDROUS FERRIC OXIDE

In this chapter we survey and synthesize available information on the major physical-chemical properties of hydrous ferric oxide (HFO). After examining the structure and composition of HFO, we present published data for surface area, site densities, and surface acid-base properties. Our main purpose is to obtain best estimates for the surface properties of HFO and provide a sense for the consistency of the corresponding experimental data.

### 5.1 STRUCTURE AND COMPOSITION

Hydrous ferric oxide, also called amorphous ferric hydroxide and amorphous iron oxyhydroxide, is the solid formed upon rapid hydrolysis of ferric iron solutions at 20 to 30°C. Four steps in this hydrolysis-precipitation process have been distinguished (Dousma and DeBruyn, 1976): (1) rapid formation of iron-hydroxo monomers and dimers; (2) reversible, rapid growth to small polymers; (3) slower formation of large polymers through the oxolation of hydroxy complexes; (4) precipitation of a solid phase. The resulting solid phase is usually completely amorphous as determined by X-ray diffraction, although a few broad reflections are sometimes observed indicating some crystalline character. Natural iron oxide material exhibiting similar diffraction patterns is often called ferrihydrite.

Freshly precipitated HFO particles are reported to be approximately spherical and quite small, with particle sizes ranging from 1 to 10 nm (van der Geissen, 1966; Avotins, 1975; Murphy et al., 1976; Tipping, 1981; van der Woude and DeBruyn, 1983; Crosby et al., 1983). This initial size distribution appears to be relatively independent of pH (van der Woude and DeBruyn, 1983). As HFO is aged, however, it coagulates and the resulting aggregates are highly

porous and sometimes micrometer sized (Avotins, 1975; Murphy et al., 1976). The water content of HFO is high because of this porosity and also because of the disordered bulk structure; thus, HFO resembles a swollen gel more than a homogeneous solid phase.

Upon precipitation of HFO, the pH of the suspension changes rapidly for the first hour and then the rate of change slows considerably. After the third or fourth hour the pH is essentially stable (Davis, 1977; Dzombak, unpublished data). Thus stable solution conditions during an experiment involving HFO are achieved only if the suspension is aged sufficiently, a minimum of 2 and preferably 4 hours. Swallow et al. (1980) demonstrated that the acid-base chemistry of HFO is noticeably different for suspensions aged 2 hours compared to suspensions aged 24 hours or longer. This difference is likely to be smaller or nonexistent for suspensions aged 3 to 4 hours. For cation or anion sorption experiments, it is adequate to allow for aging after addition of the sorbing ions if the equilibration period is of sufficient duration.

The bulk structure of hydrous ferric oxide is uncertain and its chemical composition is represented by the general stoichiometric formula  $\text{Fe}_2\text{O}_3 \cdot n\text{H}_2\text{O}$  (Cotton and Wilkinson, 1980). Thermogravimetric analyses of dried HFO samples have yielded  $n$  values between 1 and 3 (van der Geissen, 1966; Yates, 1975; Harvey and Linton, 1981; Kinniburgh and Jackson, 1982) as have analyses made with X-ray photoelectron spectroscopy (Harvey and Linton, 1981). Brown et al. (1978) note that the composition varies widely between  $\text{Fe}_2\text{O}_3 \cdot 3\text{H}_2\text{O}$  and  $\text{Fe}_2\text{O}_3$ . Measurements of the density of HFO range from 2.2 to 4.0 g/cm<sup>3</sup>, with an average near 3.5 g/cm<sup>3</sup> (van der Geissen, 1966; Murphy et al., 1975a, b, 1976; Schwertmann and Taylor, 1977).

With extended aging in aqueous solution at 20 to 30°C, HFO gradually transforms to a crystalline iron oxide, usually goethite ( $\alpha\text{-FeOOH}$ ). The rate of this transformation is faster in solutions of high Fe(III) content, high pH (> 10), and at elevated temperatures (Avotins, 1975; Murphy et al., 1976). Generally, significant amounts (2 to 10 percent) of goethite appear in HFO samples after 12 to 15 days of aging (Avotins, 1975; Crosby et al., 1983).

## 5.2 SURFACE AREA

A list of HFO surface areas measured by several techniques is given in Table 5.1. Nitrogen gas adsorption with BET analysis of the resulting isotherm is the most popular experimental method. However, the reproducibility of the method is not good with porous solids such as HFO: The results depend strongly on the outgassing procedure, and there is evidence of surface decomposition during the drying necessary for gas adsorption measurements (Yates, 1975). This surface decomposition can lead to significant underestimates of surface area. Negative adsorption measurements on porous solids may also provide low estimates for surface area due to possible restrictions on the mobility of co-ions (van den Hul and Lyklema, 1968). Thus many of the experimental measurements of the specific

TABLE 5.1 Specific Surface Areas for HFO

A (m <sup>2</sup> /g)	Method	Sources
159	BET, N <sub>2</sub> (g)	Avotins (1975)
700	Negative adsorption of Mg <sup>2+</sup> at pH 5	Avotins (1975)
434	Calculated from $\Gamma_{\text{Hg(max)}}$ assuming 59.6 Å <sup>2</sup> /Hg	Avotins (1975)
159	BET, N <sub>2</sub> (g)	Crosby et al. (1983)
234	BET, N <sub>2</sub> (g)	Crosby et al. (1983)
300 ± 50	BET, H <sub>2</sub> O	Davies-Colley (1981); Davies-Colley et al. (1984)
182	BET, N <sub>2</sub> (g)	Davis (1977); Davis and Leckie (1978)
270–335	Negative adsorption of Na <sup>+</sup>	Davis (1977)
320	BET, N <sub>2</sub> (g)	Gast et al. (1974)
250	BET, N <sub>2</sub> (g)	Pyman and Posner (1978)
250	H <sub>2</sub> O adsorbed at 19% relative humidity	Pyman and Posner (1978)
590	Ethylene glycol adsorption	Pyman and Posner (1978)
280	BET, N <sub>2</sub> (g)	Ryden et al. (1977a)
303	Glycol retention	Shuman (1977)
250	Electron microscopy	Tipping (1981)
265	BET, N <sub>2</sub> (g)	van der Geissen (1966)
257	BET, N <sub>2</sub> (g)	Yates (1975); Yates et al. (1977)
215	BET, N <sub>2</sub> (g)	Yates (1975); Yates et al. (1977)
306	BET, N <sub>2</sub> (g)	Hsi and Langmuir (1985)
720	Calculated from $\Gamma_{\text{PO}_4(\text{max})}$ assuming 0.5-nm diameter for PO <sub>4</sub>	Anderson and Malotky (1979)
257	Continuous flow method (P – E sorptometer 212D); gas adsorption, presumably	Parfitt et al. (1975)

surface area of HFO probably provide a lower bound of the actual value. A theoretical surface area of 840 m<sup>2</sup>/g for HFO is calculated (Davis, 1977) assuming 2-nm-diameter spheres and using the density of 3.57 g/cm<sup>3</sup> determined by Murphy et al. (1976). The actual surface area is thus less than 840 m<sup>2</sup>/g and more than the 200 to 300 m<sup>2</sup>/g determined by BET and negative adsorption methods. Here we use the estimate of 600 m<sup>2</sup>/g recommended by Davis and co-workers (Davis, 1977; Davis and Leckie, 1978; Luoma and Davis, 1983).

Surface densities for sorption sites on HFO are divided into two types. Type 2 sites (Table 5.3) are the total reactive sites available for sorption of protons, cations, and anions as determined from observed sorption maxima. Type 1 sites (Table 5.2) correspond to a smaller set of high-affinity cation binding sites, and the density of these sites is determined from sorption isotherms as the sorption density at which sorption becomes less than proportional to dissolved concentration (i.e., the sorption density at which the slope becomes less than 1.0 on a log-log isotherm plot). For conversions from g/L HFO to mol/L Fe, we assumed the stoichiometry  $\text{Fe}_2\text{O}_3 \cdot \text{H}_2\text{O}$  (89 g HFO/mol Fe).

TABLE 5.2 Type 1 Site Densities for HFO

$N_{s1}$ (mol/mol Fe)	Isotherm	Sources
0.005	Cd, pH = 7.5	Dzombak and Morel (1986)
0.005	Zn, pH = 6.4	Benjamin (1978, Fig. A-12)
0.005	Zn, pH = 6.5	Benjamin (1978, Fig. A-9), and with data of Kinniburgh and Jackson (1982, Fig. 2); see Dzombak and Morel (1986)
0.003–0.01	Co, pH = 8.0; for for low conc. only; possible precipitation problems above $10^{-6} M$ Co	Kurbatov et al. (1951, Figs. 1 and 3)
0.002	Pb, pH = 4.5	Benjamin (1978, Fig. A-15)
0.002–0.005	Cu, pH = 5.5	Benjamin (1978, Fig. A-6)
0.002	Cu, pH = 5.1	Benjamin (1978, Fig. A-8)
0.001–0.005	Cd, pH = 7.2	Benjamin (1978, Fig. A-3)
0.001–0.002	Cd, pH = 6.25	Benjamin (1978, Fig. A-2)
0.003–0.007	Hg, pH = 6	Avotins (1975, Fig. 16)
0.005–0.01	Zn, pH = 4.5–5.5	Kinniburgh and Jackson (1982, Fig. 3)
0.001–0.003	Zn, pH = 5.5	Kinniburgh and Jackson (1982, Fig. 2)
0.005	Ca, pH = 8.0	Kinniburgh and Jackson (1982, Fig. 2)
0.001–0.005	Ca, pH = 7–8	Kinniburgh and Jackson (1982, Fig. 3)
0.001–0.005	Sr, pH = 6.5–7.5	Kolarik (1961, Fig. 1)

TABLE 5.3 Type 2 Site Densities for HFO

$N_{s2}$ (mol/mol Fe)	Method	Sources
0.36	Tritium exchange; recalculated from $11.4/\text{nm}^2$ using the BET surface area of $215 \text{ m}^2/\text{g}$ meas- ured for the sample	Yates (1975); Yates et al. (1977)
0.91	Tritium exchange; recalculated from $20/\text{nm}^2$ using the BET surface area of $306 \text{ m}^2/\text{g}$ meas- ured for the sample	Hsi and Langmuir (1985)
0.2	$\Gamma_{\text{max}}$ for $\text{Cu}^{2+}$ , pH = 6.2	Swallow (1978, Fig. 17)
0.1–0.2	$\Gamma_{\text{max}}$ for $\text{Zn}^{2+}$ , pH = 6.5	Kinniburgh and Jackson (1982)
0.2	$\Gamma_{\text{max}}$ for $\text{Cd}^{2+}$ , pH = 7.5	Dzombak and Morel (1986)
0.18	Theoretical $\Gamma_{\text{max}}$ for $\text{Pb}^{2+}$ , hydrated; assumes that $A = 600 \text{ m}^2/\text{g}$	Luoma and Davis (1983)
0.23	Theoretical $\Gamma_{\text{max}}$ for $\text{Cu}^{2+}$ , hydrated; assumes that $A = 600 \text{ m}^2/\text{g}$	Luoma and Davis (1983)
0.24	Theoretical $\Gamma_{\text{max}}$ for $\text{Mg}^{2+}$ , hydrated; assumes that $A = 600 \text{ m}^2/\text{g}$	Luoma and Davis (1983)
0.14	$\Gamma_{\text{max}}$ for $\text{PO}_4$ , pH = 6	Ryden et al. (1977a)
0.2	$\Gamma_{\text{max}}$ for $\text{SeO}_4$ , pH = 4.5	Leckie et al. (1980, Fig. A-35)
$\geq 0.15$	$\Gamma_{\text{max}}$ for $\text{H}^+$ , pH = 4, $I = 0.25 M$	Swallow (1978)
$\geq 0.2$	$\Gamma_{\text{max}}$ for $\text{H}^+$ , pH = 3, $I = 1.0 M$	Kinniburgh and Jackson (1981)
0.5	Based on structure proposed for HFO	Kinniburgh and Jackson (1981)
0.15	$\Gamma_{\text{max}}$ for $\text{Hg}^{2+}$ ; estimated from kinetics data at pH 6.5	Avotins (1975)
0.16	$\Gamma_{\text{max}}$ for $\text{H}_3\text{AsO}_3$ , pH = 7–7.5	Ferguson and Anderson (1974, Fig. 7-5)
0.05–0.18	$\Gamma_{\text{max}}$ for $\text{H}_3\text{AsO}_3$ , pH = 7	Pierce and Moore (1982, Figs 1, 3); TOTAs = $33.4 \mu M$
0.1–0.13	$\Gamma_{\text{max}}$ for $\text{AsO}_4$ , pH = 4	Pierce and Moore (1982, Fig. 5)

The compiled estimates for the density of type 1 sites are fairly consistent, with  $N_{s1}$  ranging from approximately 0.001 to 0.01 mol/mol Fe. These estimates are sufficiently close to warrant the use of only one site density for practical purposes. In all subsequent calculations we fix the density of type 1 sites at  $N_{s1} = 0.005$  mol/mol Fe, which is the arithmetic mean of the experimental range.

estimate the density of type 2 sites as is evident in Table 5.3. The estimates for  $N_{s2}$  from the acid-base titration data of Swallow (1978) and Kinniburgh and Jackson (1981) represent the maximum extent of proton exchange observed in high-ionic-strength titrations which correspond to maximum surface charge development. They are listed as minimum estimates because surface charge accumulation may prevent complete ionization of surface groups, resulting in incomplete titration. Based on a range of estimates for  $N_{s2}$  from 0.1 to 0.3 mol/mol Fe, we use the approximate median value of 0.2 mol/mol Fe. Kinniburgh and Jackson (1981) have reported that the sorption maximum increases with pH, but the calcium sorption data at high pH upon which they base this conclusion probably include precipitation of calcium hydroxide or carbonate phase.

One might rightly wonder about the sensitivity of the results of Chapters 6 and 7 to the existing uncertainties in the values of site densities  $N_{s1}$  and  $N_{s2}$ . An error in a site density will necessarily be reflected in the corresponding equilibrium constants. For example, if  $N_{s1}$  is low by a factor of 2, the corresponding equilibrium constants for high-affinity cation sorption might be as much as 0.3 log unit too high. Thus the sorption constants associated with high-affinity sites may be off systematically by 0.3 to 0.7 log unit, while those for low-affinity sites would be within 0.15 to 0.3 log unit of the "true" value. This is only a minor problem, however, to the extent that consistency among equilibrium constants is more important than accurate values. For example, the extent of cation sorption depends on the product of surface site density and sorption constant; because it is dominated by proton competition, it also depends on some ratio of acidity and sorption constants, not their absolute values. It is only in the calculation of saturation of surface sites by one or several sorbates that systematic errors in surface site densities should lead to poor results. This difficulty can probably not be resolved since actual variations in surface site densities are to be expected

TABLE 5.4 Pristine Points of Zero Charge for HFO

PZC	Method <sup>a</sup>	Sources
8.0	PT, NaNO <sub>3</sub>	Davis (1977)
8.0	ST, NaNO <sub>3</sub>	Davis (1977)
8.0	PT, KNO <sub>3</sub>	Yates (1975)
8.0	PT, NaClO <sub>4</sub>	Ryden et al. (1977a)
7.9-8.1	PT, NaClO <sub>4</sub>	Swallow (1978)
8.0, 8.2	EM, NaCl	Tipping (1981)
8.0	ST, NaNO <sub>3</sub>	Kinniburgh et al. (1975)
8.0	ST, NaNO <sub>3</sub>	Pierce and Moore (1980)
8.05	PT, NaNO <sub>3</sub>	Dempsey and Singer (1980)
8.0	PT, NaNO <sub>3</sub>	Hsi and Langmuir (1985)

<sup>a</sup> PT, potentiometric (acid-base) titration; EM, electrophoretic mobility measurement; ST, salt titration.

among various samples of hydrous ferric oxide. In certain cases, it may be justified to adjust the values of  $N_{s1}$  and  $N_{s2}$  (keeping the ratio constant) to describe a particular sample; we have not done so.

## 5.4 POINT OF ZERO CHARGE

Pristine points of zero charge (PPZC) for HFO have been measured by acid-base titration, electrophoresis, and salt titration. As shown in Table 5.4, the results are in the range 7.9 to 8.2 with an average value of 8.0. Measurements of the PPZC by Prasad (1976) and by Kuo and McNeal (1984), which show markedly lower values, are specifically excluded because of long aging times and hence the possibility of transformation of HFO to goethite.

## 5.5 SURFACE ACID-BASE CHEMISTRY

Reproducible acid-base titrations for hydrous ferric oxide are difficult to achieve (Davis, 1977; Swallow, 1978; Yates, 1975), and probably for this reason few HFO titrations have been published (see Table 5.5). Both Yates (1975) and Davis (1977) observed significant hysteresis in conducting consecutive acid and base titrations of HFO. Acid titration curves were shifted as much as 0.4 pH unit lower than base titration curves in the pH range 6 to 9.

The optimal surface acidity constants extracted from the available data sets are reported in Table 5.6. As noted in Appendix A, Davis' data were obtained in an acid titration, while the other data sets correspond to base titrations. Two other sets of HFO titration data were excluded from this analysis because of a slow titration rate (Pyman and Posner, 1978) and overaging of the HFO sample (Prasad, 1976).

The high residual sum of squares associated with some of the data sets in Table 5.6 is attributable primarily to an insufficient number of titration data at high pH, above the PPZC. With a more balanced distribution of data above and below the PPZC, much lower residuals are obtained from nonlinear regression. Experimental data and calculated titrations are presented in Figures 1T1 to 1T10: Solid lines represent optimum fits of individual experiments; dashed lines represent fits corresponding to the best overall estimate of acidity constants. The fits are quite good in most cases. In the four cases with high residuals (Figures 1T2, 1T3, 1T7, and 1T10), the limited high-pH data are not fit closely, but the overall fits are certainly adequate.

The weighted averages for  $\log K_{a1}^{int}$  and  $\log K_{a2}^{int}$  are given in Table 5.7 along with confidence intervals for these best estimates. At the 95 percent confidence level,  $pK_{a1}^{int} = 7.29 \pm 0.10$  and  $pK_{a2}^{int} = 8.93 \pm 0.07$ . The available data are fairly consistent, for even at the 99 percent confidence level the deviations from the best estimates are only about 0.15 log unit.

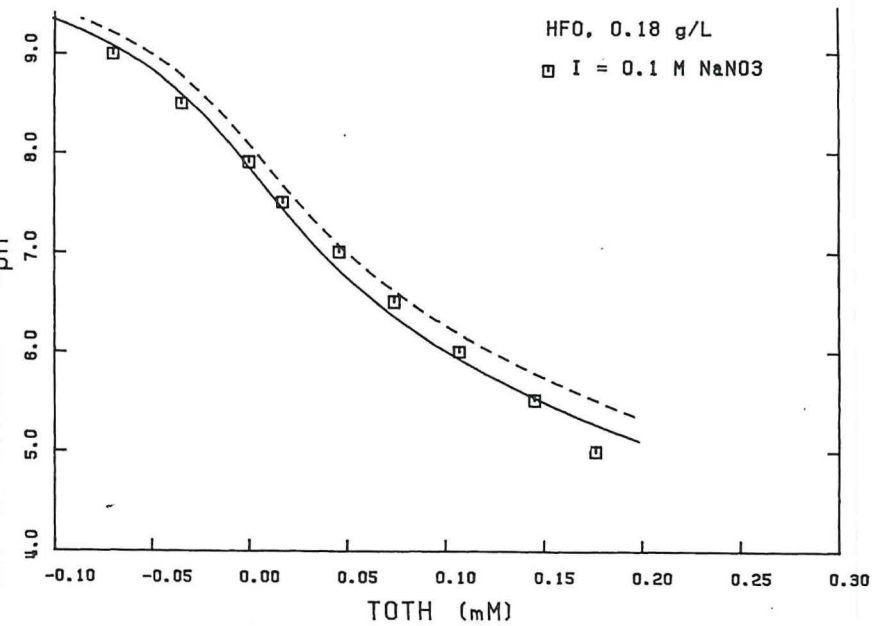


Figure 1T1.

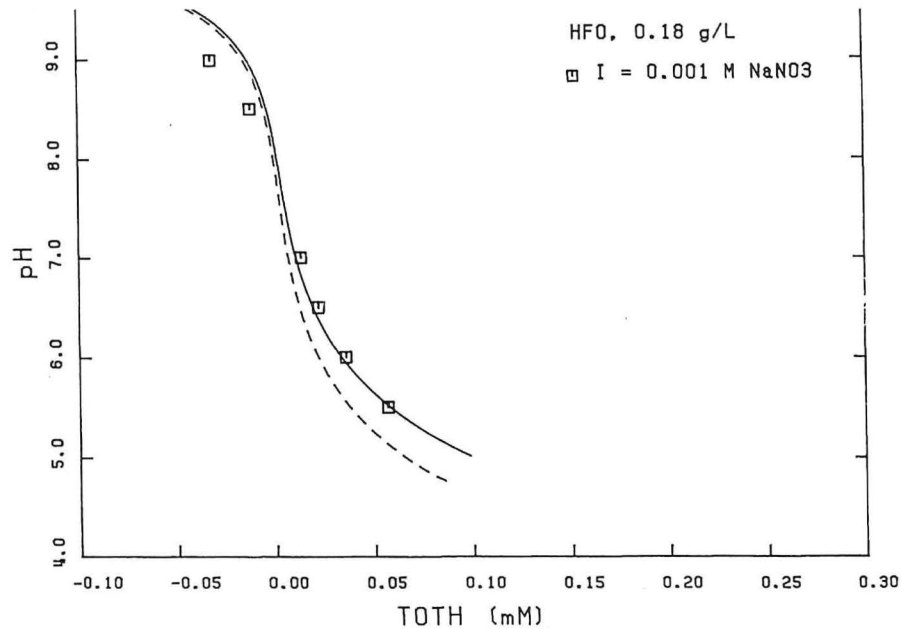


Figure 1T3.

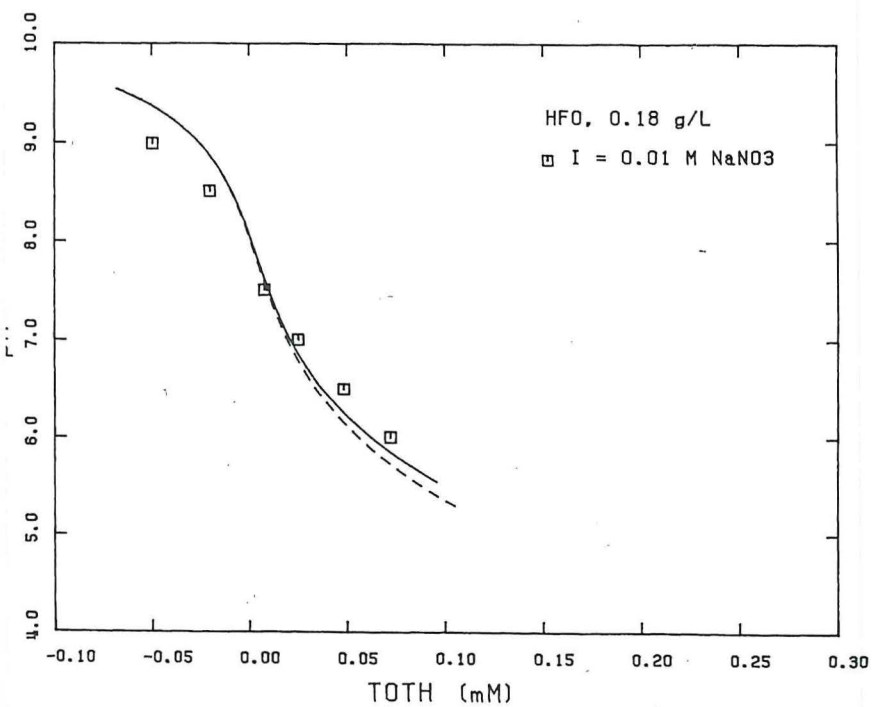


Figure 1T2.

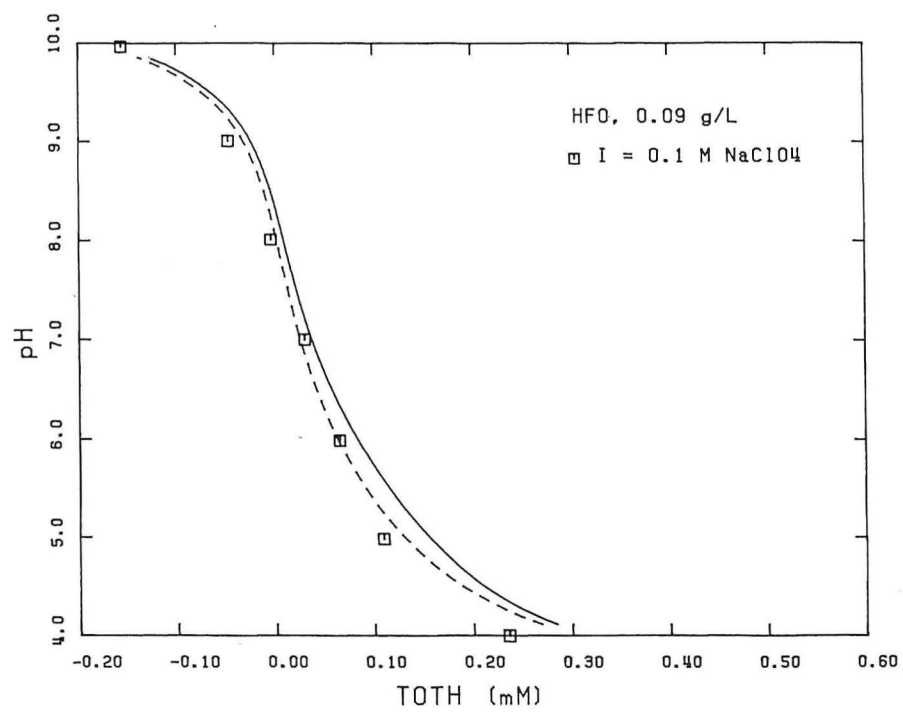


Figure 1T4.

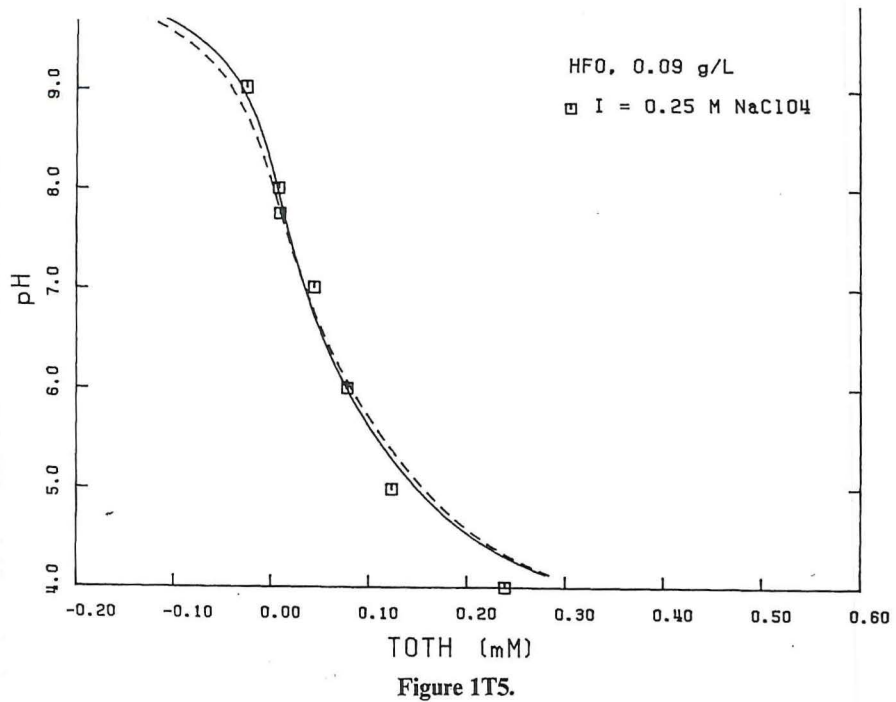


Figure 1T5.

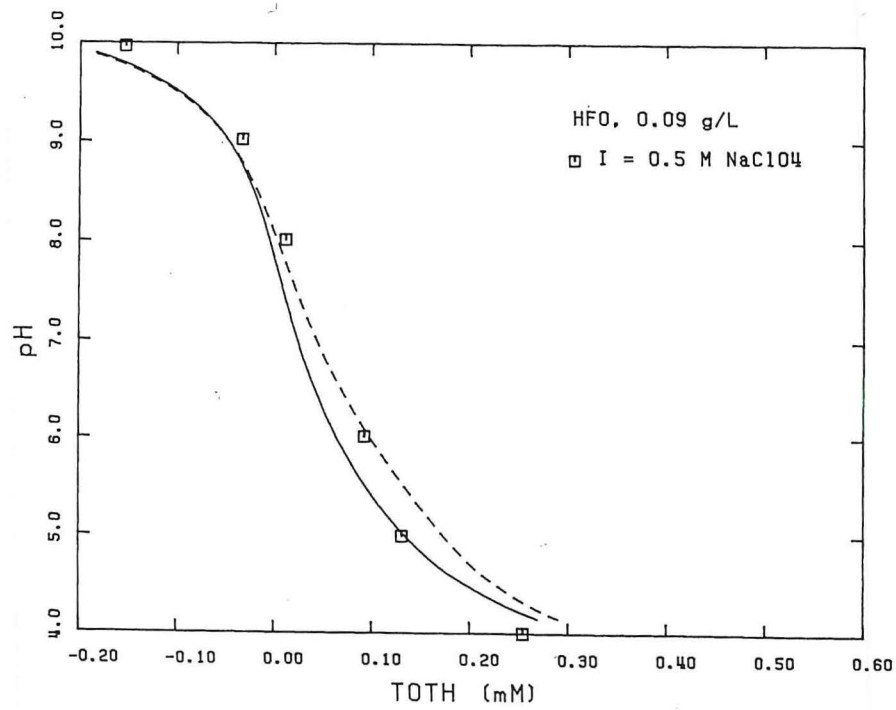


Figure 1T6.

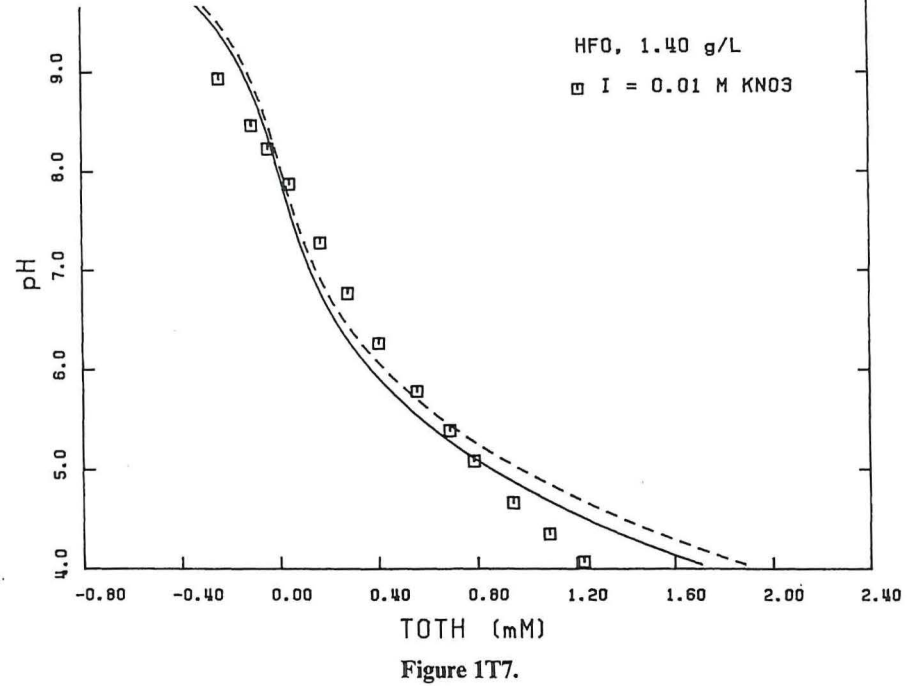


Figure 1T7.

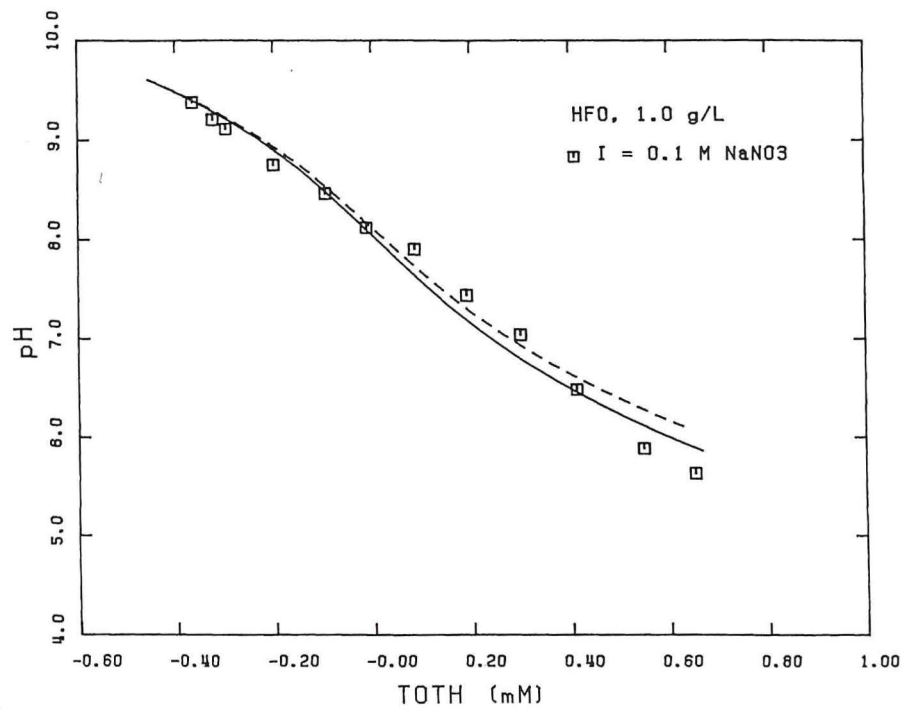
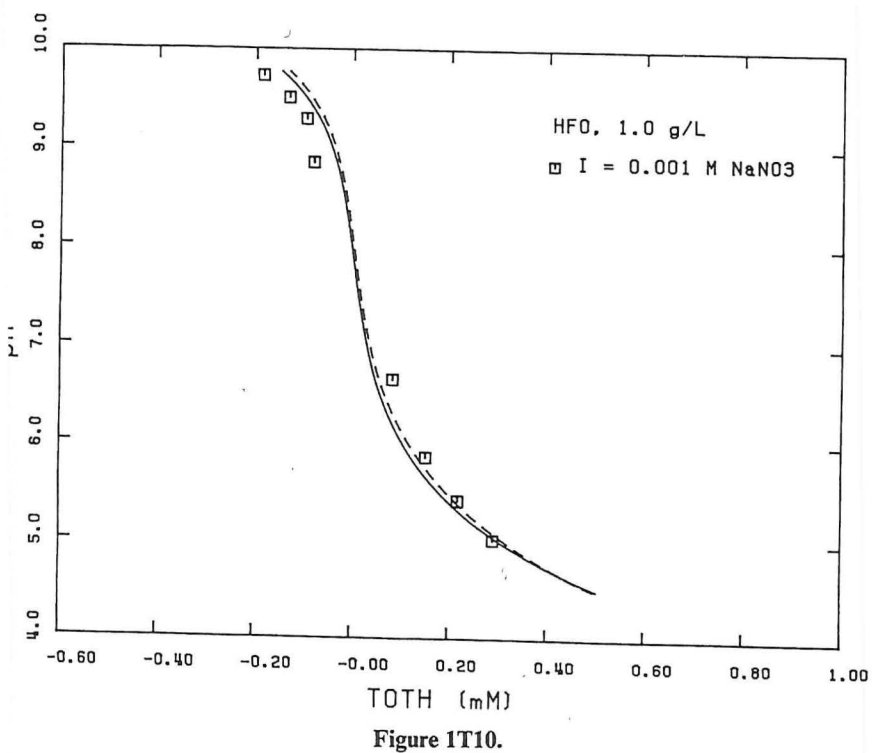
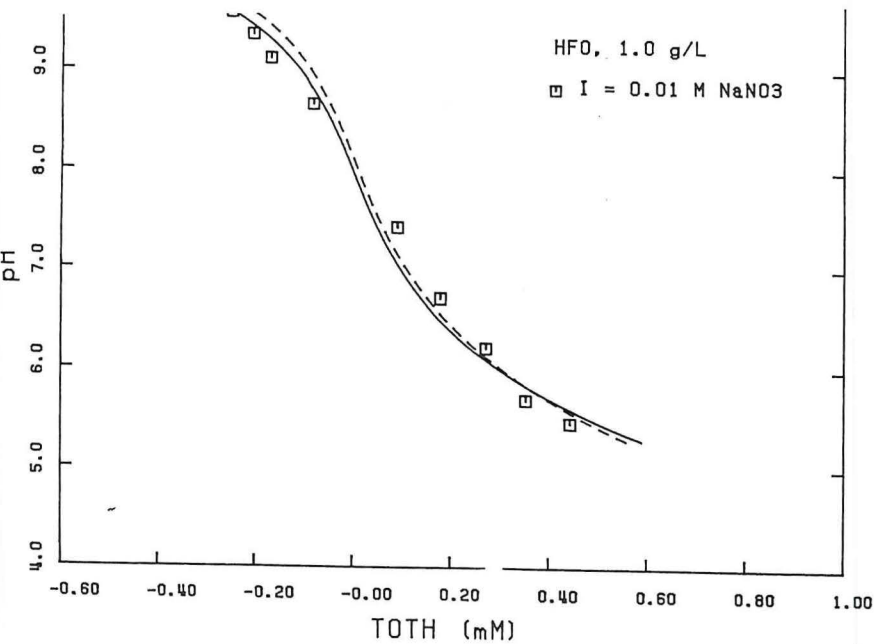


Figure 1T8.



ID	Source	Medium	Data Set
1T1	Davis (1977)	0.1 M NaNO <sub>3</sub>	Fig. 4.2
1T2		0.01 M NaNO <sub>3</sub>	
1T3		0.001 M NaNO <sub>3</sub>	
1T4	Swallow (1978)	0.1 M NaClO <sub>4</sub>	Fig. 4
1T5		0.25 M NaClO <sub>4</sub>	
1T6		0.5 M NaClO <sub>4</sub>	
1T7	Yates (1975)	0.01 M KNO <sub>3</sub>	Fig. 6.20
1T8	Hsi and Langmuir (1985)	0.1 M NaNO <sub>3</sub>	Fig. 6
1T9		0.01 M NaNO <sub>3</sub>	
1T10		0.001 M NaNO <sub>3</sub>	

TABLE 5.6 HFO Intrinsic Surface Acidity Constants

ID	$pK_{a1}^{int}$	$\sigma_{\log K}$	$pK_{a2}^{int}$	$\sigma_{\log K}$	SOS/DF
1T1	7.03	0.035	8.74	0.065	9.1
1T2	7.57	0.038	8.74 <sup>a</sup>	0.15 <sup>b</sup>	66.3
1T3	8.20	0.045	8.74 <sup>a</sup>	0.15 <sup>b</sup>	87.3
1T4	7.69	0.048	9.25	0.118	21.0
1T5	7.17	0.032	9.51	0.095	15.8
1T6	6.63	0.033	9.10	0.065	10.8
1T7	7.10	0.026	8.89	0.045	75.8
1T8	7.08	0.028	9.01	0.034	18.8
1T9	7.58	0.110	8.40	0.126	22.4
1T10	7.54	0.040	8.40 <sup>a</sup>	0.15 <sup>b</sup>	71.6

<sup>a</sup>Fixed at this value, based on result for 1T1. Convergence not possible unless one surface acidity constant fixed.

<sup>b</sup>Fixed at this value by convention.

TABLE 5.7 Best Estimates for HFO Acidity Constants

Best-Estimate $K$	Confidence Level	$pK_a^{int}(-)$	$pK_a^{int}(+)$
$\log \overline{K_{a1}^{int}} = -7.29$	0.99	7.15	7.43
	0.95	7.19	7.38
	0.90	7.21	7.36
	0.80	7.23	7.35
$\log \overline{K_{a2}^{int}} = -8.93$	0.99	8.83	9.02
	0.95	8.86	9.00
	0.90	8.87	8.98
	0.80	8.89	8.97

... between the two acidity constants, the number of positively charged sites are equal (in the absence of specific cation or anion adsorption) and the surface is uncharged. As discussed in Chapter 2, the point of zero charge is given by the average of the two  $pK_a$  values:

$$PPZC = 0.5(pK_{a1}^{int} + pK_{a2}^{int}) \quad (5.1)$$

Substituting the best estimates for  $pK_{a1}^{int}$  and  $pK_{a2}^{int}$  from Table 5.7 yields  $PPZC = 8.1$ , which is in close agreement with measured values (see Table 5.4). For the sake of consistency, it is important to remember that the intrinsic acidity constants in Table 5.7 may have to be corrected for ionic strength effects when employed in chemical equilibrium calculations. If fixed proton activity (pH) calculations are performed, the intrinsic acidity constants (modified by the Debye-Hückel term) are used. However, if chemical equilibrium calculations are performed on a concentration basis (typically, molar), the solution activity coefficient for  $H^+$  must be included to modify the intrinsic acidity constants. That is,

$$K_{a1}^{int} = \frac{(\equiv FeOH^o)\{H^+\}}{(\equiv FeOH_2^+)} P = \frac{(\equiv FeOH^o)\gamma_H(H^+)}{(\equiv FeOH_2^+)} P \quad (5.2)$$

$$K_{a2}^{int} = \frac{(\equiv FeO^-)\{H^+\}}{(\equiv FeOH^o)} P = \frac{(\equiv FeO^-)\gamma_H(H^+)}{(\equiv FeOH^o)} P \quad (5.3)$$

where  $P = \exp(-F\Psi/RT)$ . We have been careful about correcting  $K_{a1}^{int}$  and  $K_{a2}^{int}$  with  $\gamma_H^{-1}$  in calculating, on a concentration basis, the data fits shown in Figures 1T1 to 1T10 and throughout Chapters 6 and 7.

# 6

## CATION SORPTION ON HYDROUS FERRIC OXIDE

Sorption equilibrium constants extracted from available data for cation sorption on hydrous ferric oxide are reported in this chapter. There are separate sections for each of the cations investigated, and each of these sections contains the following: (1) the sources of the sorption data used for parameter extraction, (2) the data sets rejected, (3) the surface complexation reactions used in fitting the data, (4) the optimal equilibrium sorption constants for each data set, (5) the best overall estimates (and associated confidence intervals) for the sorption constants, and (6) a plot of each data set along with the optimal fit (solid line) and the fit corresponding to the best overall estimate of sorption constants (dashed line). A key to the identification code employed in the tables and figures for the various data sets is provided in Table 4.5. Comments on particular data sets used or rejected are given in Appendix A. Table 6.0 lists the solution complexation reactions considered in fitting the various cation sorption data sets; the aqueous chemistry of the cations investigated is adequately described elsewhere [e.g., Cotton and Wilkinson (1976, 1980), Baes and Mesmer (1976), and Smith and Martell (1976)].

In the generalized two-layer model, cation sorption is represented as surface complexation on two site types with surface precipitation at high cation concentrations (see Chapter 2). With the exception of zinc and mercury, the sorption constants reported in the following pages are for surface complexation only. To include the effects of surface precipitation, the reported *surface complexation constants* must be adjusted by a constant factor, namely the solubility product for ferric hydroxide ( $K_{spFe} = 10^{-2.5} = \{Fe^{3+}\}\{H^+\}^{-3}$ ), and a surface precipitation reaction for the hydroxide of the sorbing cation must be added ( $K_{spM} = \{M^{2+}\}\{H^+\}^{-2}$ ; see Chapter 2). This conversion of surface complexation constants to surface precipitation constants, though easy to